

Investigation on Stress Corrosion Cracking Behavior of Welded High Strength Low Alloy Steel in Seawater Containing Various Dissolved Oxygen Concentrations

Huixia Zhang^{1,*}, ‡ Xiaodong Wang^{1,2,‡}, Ruiling Jia², Jian Hou¹, Weimin Guo¹

¹ Science and Technology on Marine Corrosion and Protection Laboratory, Luoyang Ship Material Research Institute, Qingdao (China)

² Inner Mongolia University of Technology, Key Laboratory for superlight materials of Inner Mongolia, Huhhot (China)

*E-mail: zhanghx@sunrui.net

‡ These authors contributed equally.

Received: 16 November 2012 / Accepted: 9 December 2012 / Published: 1 January 2013

In this report, the susceptibility to stress corrosion cracking of welded high strength low alloy (HSLA) steel, immersing in seawater with different dissolved oxygen (DO) concentrations at 5°C with the potential of -1.2 V, was investigated by slow strain rate test (SSRT). The SSRT results indicate that there is a lower elongation and percentage reduction in area with lower DO concentration. Fracture surface morphology showed that quasi-cleavage fracture and short necking appeared at higher DO level, which was revealed by scanning electron microscopy (SEM) and optical microscopy. The polarization resistance reduced during the SSRTs with an increase in DO concentration of seawater, using electrochemical impedance spectroscopy (EIS). It is illustrated that the SCC susceptibility of welded HSLA steel increases with the increment of DO concentration in seawater, because higher DO content enhances the oxygen reduction reactions on metal surfaces and accelerates the metal anodic dissolution rate at the crack tips and on crack walls.

Keywords: welded high strength low alloy steel, dissolved oxygen, seawater, slow strain rate test, electrochemical impedance spectroscopy

1. INTRODUCTION

High strength low alloy (HSLA) steel is extensively used in advanced maritime facilities like offshore and navy ships, on account of the high strength and easy welding properties [1-5]. Recent studies on the stress corrosion cracking (SCC) behavior of HSLA steel showed high SCC susceptibility due to the high strength [6-12]. Furthermore, application of these alloys requires welding

and joining procedures to be developed. The welding process inevitably causes changes in the original microstructure of the alloy due to welding thermal cycles. These micro structural changes can affect the localized corrosion behavior of the alloy. Additionally, welded joints bring some amount of welding defects into a material during welding, and residual stresses are usually present in welded components [1,13-26]. Thus a risk of SCC will occur during service. The main hazardous risk is that SCC always cause unexpected brittle failures without any externally visible indications, which will significantly restrict its application in marine environment. The cathodic protection system has been used to protect the HSLA steel from corrosion and extend its service life in the offshore and navy ships. In fact, over protection often occurs during cathodic protection, which may cause much more serious SCC problems [27-29]. Thus the research of SCC behavior of welded HSLA steel under cathodic potential is of great significance.

The scientific exploration of the ocean depths is now proceeding in deep sea environment, and has urged the need to study the behavior of HSLA steel in deep oceans. There is lower dissolved oxygen (DO) concentration in 300~1000m deep sea than the shallow sea [30]. Furthermore the reduction of DO directly affect the corrosion rate of HSLA steel as its corrosion process is determined by oxygen reduction reaction which is controlled by oxygen diffusion in seawater [31]. Once all other factors are held constant, the corrosivity of seawater increases as an increase in temperature. Corrosion rates are usually higher in warm shallow sea than cold deep sea, as the electron-transfer rate constant and oxygen diffusion respond immediately to the temperature change. Furthermore the saturation concentration of DO increases while temperature decreases and the effects of DO on the corrosion rate are often stronger than that of temperature [32]. So that it is necessary to study SCC behaviors of welded HSLA steel.

The effect of DO in seawater on SCC of HSLA steel has been studied little until now. However the effect of DO on crack growth has been mentioned when SCC behaviors of stainless steel are investigated in high temperature pure water. Lu [33-34] has studied the SCC growth kinetics for a cold worked 316L stainless steel which was continuously monitored in high purity water at DO concentrations(2~7.5 ppm) and found that the steady state crack growth rate increases with increasing DO concentration. Turnbull [35]has made in-situ measurements of the crack-tip potential in a fatigue-precracked compact tension specimen of a 3 % NiCrMoV steam turbine disc steel immersed in simulated steam condensate environments with very low oxygen concentration (1~1500 ppb) at 90°C. The results showed that both corrosion potential and crack-tip potential shift positively with increasing DO concentration. However results mentioned above were all obtained at very low DO level of pure water. The effect of DO concentration on SCC behaviors of welded HSLA steel in seawater has not been known until now, furthermore this is so importance on application in deep ocean. Thus it is worthwhile to study SCC behavior of welded HSLA steel in seawater containing various DO concentrations under over protected potential at 5°C. To achieve this objective scanning electron microscopy (SEM) and optical microscopy were used to examine fracture, and electrochemical impedance spectroscopy (EIS) to analysis the SCC process.

2. EXPERIMENTAL PROCEDURE

2.1 Material

HSLA steel plate with minimum yield strength 710 MPa was used in this work. The steel plates were welded by manual arc welding which is efficient welding technique. The base metal should be preheated to 150 °C, and used two types of filler wire at different current to weld: a filler wire of 3.2 mm diameter at 110 A, and the other wire of 4.0 mm at 130 A.

The tensile test specimens were 156 mm in length which were machined to give a gauge length of 30mm and a diameter of 5 mm. The butt weld was 20 mm in width which located in the center of the gauge length. The structural diagram of specimen is shown in Fig1.

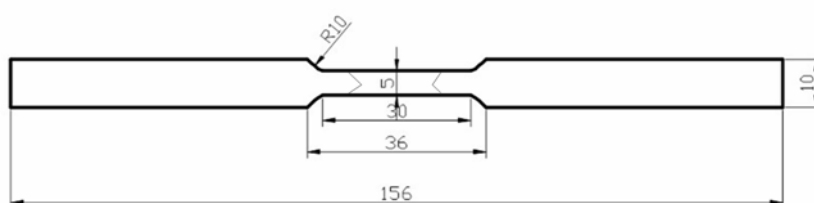


Figure 1. The sketch map of specimen

Before conducting the tests, the specimens were ground with 320, 600, 1200, and 2000 grit SiC papers, cleaned in distilled water, degreased with acetone, and coated with 704 # silica gel so that only the gauge length was exposed to the test solution.

2.2 Slow strain rate test

Slow strain rate tests were carried out by using electronic universal testing machine model CMT 5305 at a constant strain rate of $8.33 \times 10^{-8} \text{ s}^{-1}$ in seawater with various DO content under an applied potential of -1.2 V. The seawater temperature was controlled at 5 °C by using thermostatic bath (DC-2015), while the DO content was controlled between 2~8 mg/L by aerating mixed gas of oxygen and nitrogen into seawater, which was pumped into electrolytic cell continually in cycle by circulating pump.

After failure, the susceptibility to SCC was expressed in terms of percentage reduction of area (ROA), fracture time (T_f) and elongation (E_f), which were calculated by following expression:

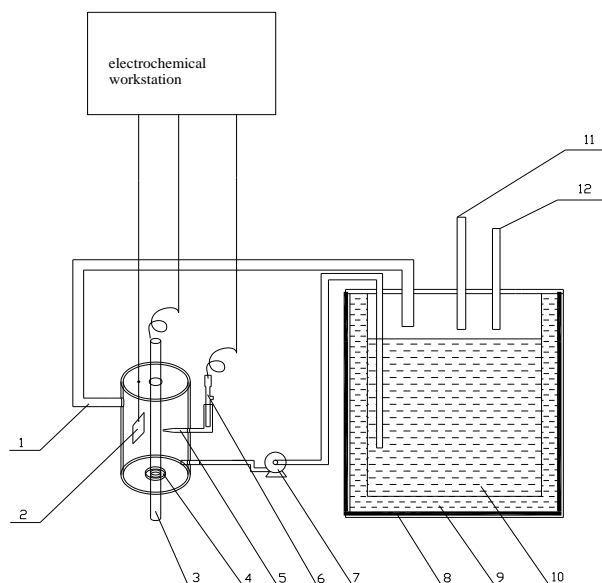
$$ROA = \frac{A_i - A_f}{A_i} \times 100\% \quad (1)$$

$$E_f = \frac{L_i - L_f}{L_i} \times 100\% \quad (2)$$

A_i and A_f are the initial and final area of cross section of gauge length, respectively. L_i and L_f are the initial and final length of gauge length, respectively.

2.3 Electrochemical measurements

The electrolytic cell used a organic home-made glass cylinder, closed by upper and lower stoppers, through which the ends of the specimen protruded. The sketch map of the cell and measurement system was shown in Fig. 2.



1.draining tube 2.Pt electrode 3.specimen 4.sealing device 5.Luggin capillary 6.saturated calomel electrode 7.circulating pump 8. thermostatic bath 9.running water 10.test solution 11.filling nitrogen 12.filling oxygen

Figure 2. The sketch map of the cell and measurement system

EIS measurements were performed by electrochemical workstation (ACM Field Machine Serial No 1527 made in England). Ten millivolts were applied as AC signal around the applied potential of -1.2 V. The frequency range was from 10^5 Hz to 10^{-2} Hz. A typical three electrode system, consisting of the specimen as the working electrode, Pt sheet as the counter electrode and saturated calomel electrode as a reference electrode.

2.4 Scanning electron microscopy and Optical Microscopy

In order to observing micro-morphology of failed specimens which were cut 1cm away from the fractured region, washed with acetone by ultrasonic washer to wipe off contamination, and then washed with distilled water before drying with hair drier.

The fracture surface was inspected by using a scanning electron microscopy model FEI/Philips XL30 with an accelerating voltage of 20.0 kV. Samples were attached on the top of an aluminum

stopper by means of carbon conductive adhesive tap in order. The sampling area is concentrated at the ductile fracture zone.

The fracture profile-surface of failed specimens were polished using different grade of emery papers followed by washing with distilled water and acetone and then drying with hair drier. The metallogical structure were inspected by using optical microscopy model LEICA DMI 5000 M after etching with solution containing 500 mL HCL and 3.5 g hexamethylenetetramine and 500 mL distilled water.

3. RESULTS AND DISCUSSION

3.1 Slow strain rate test

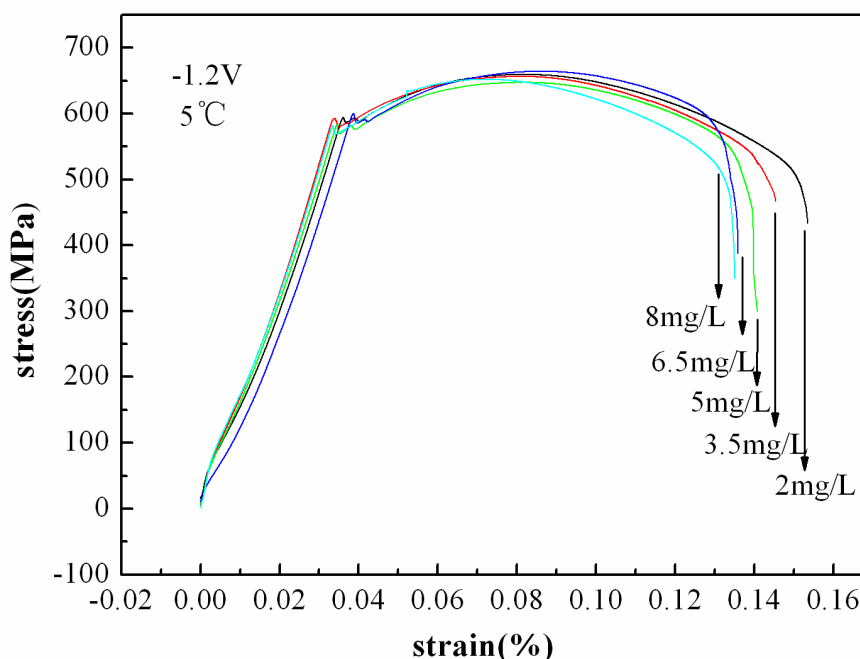


Figure 3. Stress-strain curves of specimens obtained from SSRT tests in seawater with different DO concentrations

Table 1. The yield strength (σ_s) and tensile strength (σ_b) of specimens obtained from SSRT tests in seawater with different DO concentrations

	2mg/L	3.5mg/L	5mg/L	6.5mg/L	8mg/L
σ_s (MPa)	592	584	580	585	568
σ_b (MPa)	659	655	647	653	651

SSRTs have been performed to investigate mechanical properties of welded HSLA steel in seawater with different DO concentrations. Stress-strain curves of the specimens obtained from the

SSRTs in seawater with various DO concentrations at 5 °C under -1.2 V potential are shown in Fig. 3, and the yield strength and tensile strength in Table 1. The gradual decrease of specimens strain is observed with the increase of DO concentrations. The yield strength fluctuated from 568 MPa to 590 MPa and tensile strength fluctuated from 647 MPa to 663 MPa. It indicated a little decrease as an increase in DO content. As shown in Fig.4, for the specimens tested in seawater, T_f shortened, E_f and ROA reduced when DO concentrations increased from 2.0 mg/L to 8 mg/L gradually.

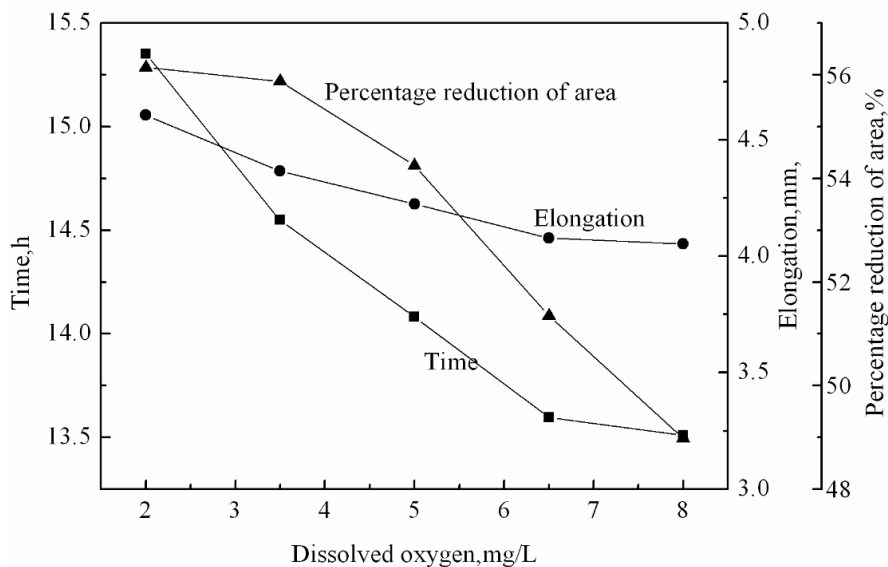


Figure 4. Fracture time, elongation and percentage reduction of area of specimens after SSRT tests in seawater with different DO concentrations

The susceptibility to SCC is indicated by a decrease in mechanical properties, such as strain values before failure, tensile strength, ROA and E_f [36]. The SCC susceptibility of the tensile specimens is higher while tested in seawater with higher DO concentration.

3.2. Morphologies for the fracture specimens

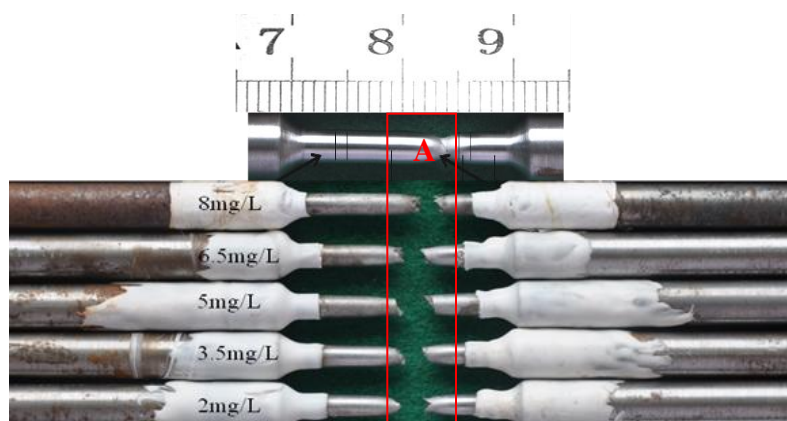


Figure 5. The digital photo of failure specimen

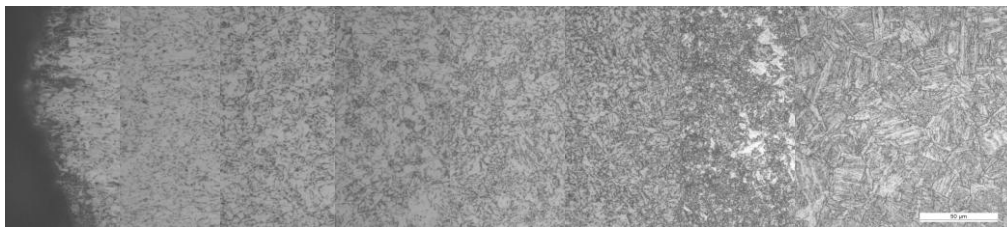


Figure 6. metallurgical structure of cross-section surface of failure specimen (500×)

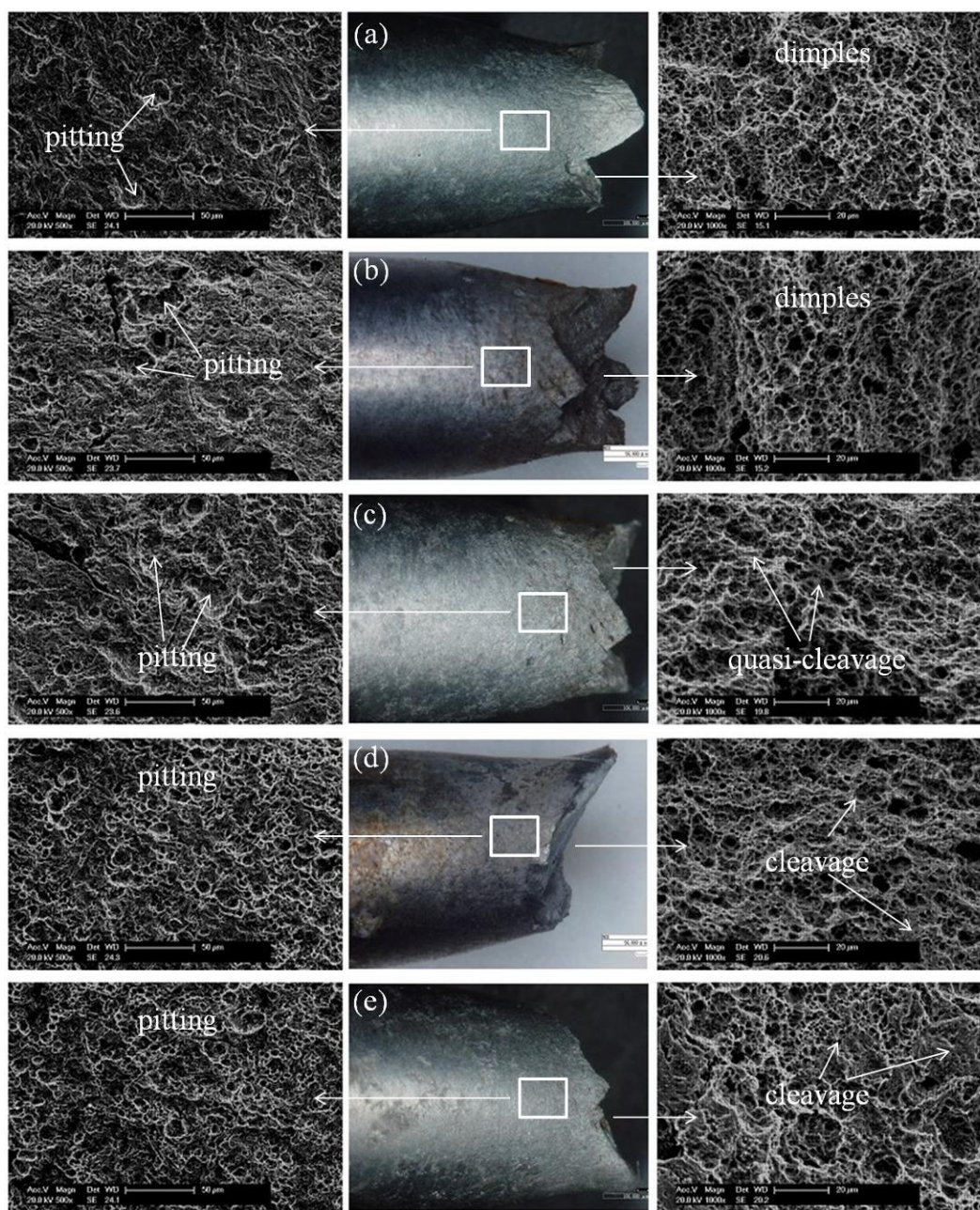


Figure 7. The fracture profile-surface and fracture surface of specimens seawater with different DO concentrations in circulating seawater (a)2mg/L (b)3.5mg/L(c)5mg/L(d)6.5 mg/L(e)8 mg/L

The digital photo of failure specimens are shown in Fig. 5, the failure almost occurred near the center line of guage length. It was found that failure occurred most far away from the center line when

test in seawater with 8 mg/L DO concentration. The metallurgical structure of cross-section surface of failure specimens are shown in Fig. 6. Ferrite and granular bainite which are the character phase composition of weldment were observed in fracture zone of specimens. It could be decided that failure taken place in the welding line zone. It implied that welding zone had the worst resistance to SCC comparing to the parent material and heat affected zone of steel joints and welding defect maybe existed in the welding zone.

Fig. 7 shows SEM images of the fracture profile-surface and fracture surface of steel specimens obtained from seawater with different DO concentrations. It was examined from the fracture profile-surface images that pitting reduced with a decrease in DO concentration, which confirm that the DO did in fact aggravate corrosion. Moreover, it was observed from SEM images of fracture surface in Fig. 7 that the reduction of dimples accompanied by a change in fracture mode by DO concentration decreasing. For fracture surface of specimens tested at 2 mg/L and 3.5 mg/L DO content abundant of dimples were found, at higher DO concentrations, quasi-cleavage and cleavage fracture were observed on fracture surface, which is corroborated by very little necking in the specimens.

3.3. Electrochemical Measurements

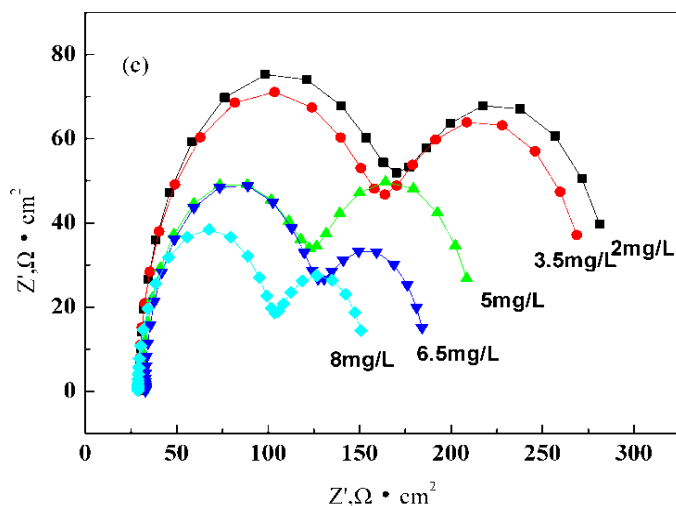


Figure 8. Electrochemical impedance Nyquist plots of specimens in seawater with different DO concentrations at (a) 2h (b) 6h (c) 10h during SSRT tests

Electrochemical impedance Nyquist plots of specimens obtained from seawater with different DO concentrations during SSRT tests at 2 h, 6 h and 10 h respectively were shown in Fig. 8. Nyquist plots come as an arc of very large diameter in the high frequency range and an arc of smaller diameter in the lower frequency range respectively, two time constants indicate that local corrosion, e.g. cracks, pits, had happened [37]. Thus an equivalent circuit model shown in Fig. 9, was proposed to describe the corrosion process of specimens in seawater during SSRT tests. In this circuit, R1 is solution resistance, CPE1 is the rustyscale capacitance, R2 is the rustyscale resistance, CPE2 is the double layer capacitance and R3 is the charge transfer resistance. The two semi-circles in the Nyquist diagram

represented characteristic of the rustyscale resistance (R_2) and capacity (CPE_1) at the high frequency range and characteristic of the charge-transfer resistance (R_3) and the capacity (CPE_2) in the low frequency range [38].

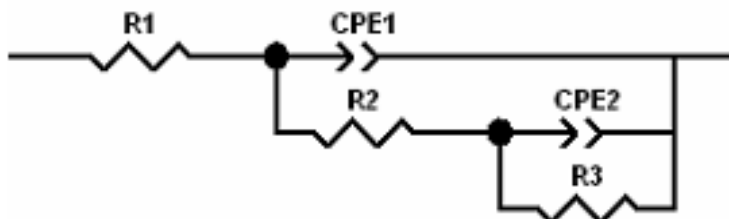


Figure 9. equivalent circuit model

The size of the semi-circles became larger as a decrease in DO concentration of seawater at different moment of the SSRT tests, for instance 2h, 6h, 10h, which meant that the impedance at high DO concentrations were far lower. A decrease of impedance with increasing of DO concentrations in bulk seawater during lower frequency range corresponds to the anodic reaction concentrating at crack tips and on the crack walls that generate a lower charge transfer resistance and accelerate the dissolution of new surface on the crack wall. Moreover, during higher frequency range, a decrease of rustyscale resistance corresponds to a smaller impedance, which is conducted by consumption of rustyscale on the surrounding surface near the cracks. A higher consumption of oxidizing species illustrates a higher crack growth rate [38], thus at higher DO concentrations anodic dissolution of steel at crack tips and also on the crack walls would be accelerated, as the oxygen diffusion through corrosion products to steel surface [39]. The initiation of cracks were often associated with pitting which derived from defects, inclusions and interpositions on steel surface. Because to increase bulk seawater DO concentration is to increase the corrosion rate of pitting [39], the susceptibility to SCC behaves remarkably with an increase in DO concentration.

In this paper polarization resistance (R_p) value is the sum of R_2 and R_3 obtained from EIS. R_p can be used to evaluate the corrosion resistance of specimens. It is generally believed that a system with higher R_p was less susceptible to be agressed and had better resistance to corrosion. Fig.10 shows the time-dependent change in the R_p calculated from Nyquist plots. R_p decreases slightly with the DO variation from 2 mg/L to 3.5 mg/L and decreases faster while DO concentration changed more than 3.5 mg/L. These imply that the worse corrosion resistance as DO arising. The change in R_p values agrees with the Nyquist plots shown in Fig. 8 at either test time. The higher R_p values are entirely consistent with lower DO concentrations, as the corrosion rate is determined by the oxygen reduction reaction rate which controlled by oxygen diffusion rate. As shown in Fig.11, anodic reaction (5) is concentrated at crack tips and on the crack walls, and cathodic reaction (3) (4) occurred on the surrounding surface near cracks.

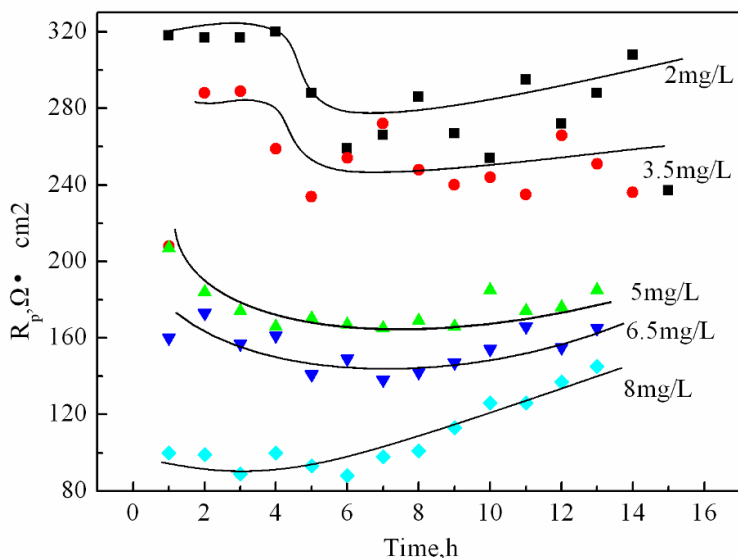


Figure 10. The polarization resistance of the high-strength low-alloy steel in seawater with different DO concentrations during SSRT tests

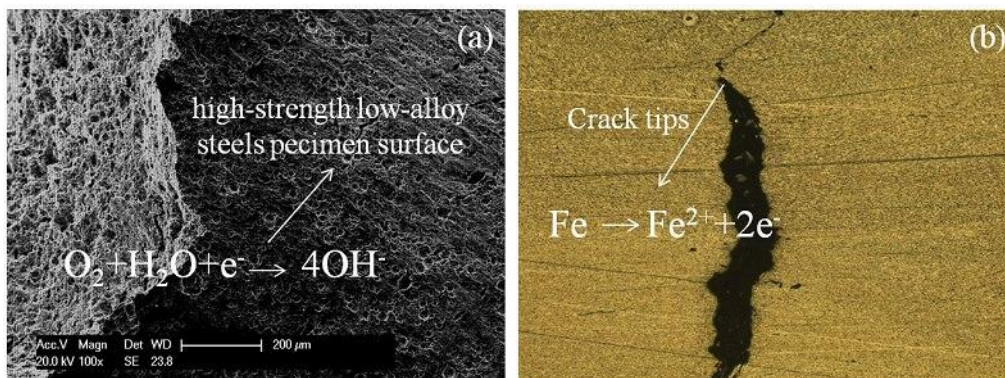
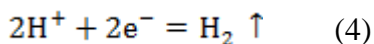
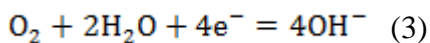


Figure 11. SEM (a) and optical microscopy (b) images at the crack tip

Because the cathodic reaction (3) (4) rate (R_c) is determined by oxygen diffusion rate through bulk seawater and rustyscale, the anodic dissolution (5) corresponds to the pH value of solution in the cracks. As OH^- ions concentration increase with increase in R_c , the H^+ ions concentration in the cracks (occluded cells) arises, and this lead to smaller pH value which accelerates anodic dissolution of steel at crack tips and on crack walls [40]. Cathodic reaction is mainly accomplished as in this reaction (Fig 10(a)).



The anodic reaction is the dissolution of Fe that is shown in Fig.10 (b)

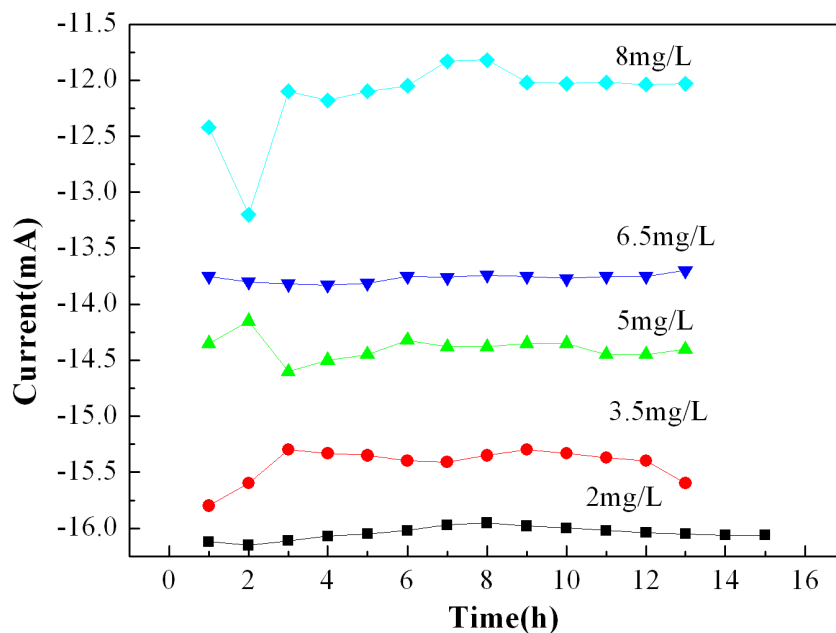
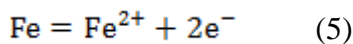


Figure 12. The corrosion current under applied potential of -1.2V of HSLAS in simulated deep-sea seawater with different DO concentrations during SSRT tests

As shown in Fig.12, the corrosion current of specimens increase with DO concentration increasing, which indicates that higher DO concentration enhanced the anodic dissolution of specimens. It is in accordance with the EIS and SSRT test results, and all the results above indicate that the susceptibility to SCC of the welded HSLA steel increase with DO concentration in seawater increasing.

4. CONCLUSION

The failure of the welded HSLA steel tensile specimens occurred in weld zone which was the weakest area of the joints. The mechanical properties decreases as an increase in DO concentration of seawater. The susceptibility to SCC became more notable with increase of DO concentrations in seawater at 5°C. It is considered that the higher DO concentrations enhanced the oxygen reduction reaction rate on steel surfaces and accelerated the metal anodic dissolution rate at the crack tips and on the crack walls of welded HSLA steel.

References

1. J. Ćwiek. *Mater. Manuf. Eng.*, 20 (2007), 223
2. N. Eliaz, A. Shachar., B. Tal., D. Elieze, *Eng. Failure Anal.*, 9 (2002), 167
3. J.Ćwiek, K. Nikiforov, *Corros. Sci.*, 40 (2004), 831.

4. H. Y. Liou, R. I. Shieh, F. I. Wei, S. C. Wang, *Corrosion*, 49 (1993), 389
5. S.P. Lynch, *Eng. Failure Anal.*, 1 (1994), 77
6. J. Ćwiek, *J. Mater. Process. Technol.*, 164–165 (2005), 1007
7. N. Eliaz, A. Shachar, B. Tal, D. Eliezer, *Eng. Failure Anal.*, 9 (2002), 167
8. C. L. Briant, S. K. Banerji, *Int. Met. Rev.*, 23 (1978), 99
9. C. D. Beachem, *Metall. Trans.*, 3 (1972), 51
10. H.Y. Liou, R. I. Shieh, F. I. Wei, S. C. Wang, *Corrosion*, 49 (1993), 98
11. P. Buckley, B. Placzankis, L. Lowder, I. G. Brown, *Surf. Coat. Technol.*, 49 (1991), 3
12. L. Vehovar, *Mater. Corros.*, 45(1994), 354
13. J. Wang, Y. Li, *Mater. Sci.*, 26 (2003), 295
14. S. Roy, J. W. Fisher, B. T. Yen, *Int. J. Fatigue*, 25 (2003), 9
15. A. F. Blom, *Int. J. Fatigue*, 17 (1995), 485
16. L. P. Borrego, J. T. B. Pires, J. M. Costa, J. M. Ferreira, *Eng. Failure Anal.*, 14 (2007), 1586
17. J. Grum, J. M. Slabe, *Surf. Coat. Technol.*, 180-181(2004), 596
18. J. Grum, J. M. Slabe, *Appl. Surf. Sci.*, 208-209(2003), 31
19. J. B. Li, X. Hou, M. S. Zheng, J. W. Zhu, *Int. J. Electrochem. Sci.*, 2 (2007) 607.
20. X. Cheng, J. W. Fisher, H. J. Prask, T. Gnäupel-Herold, B. T. Yen, S. Roy, *Int. J. Fatigue*, 25 (2003), 1259
21. K. Y. Bae, T. H. Lee, K. C. Ahn, *J. Mater. Process. Technol.*, 120(2002), 458
22. A. Allen, M. T. Hutchings, G. G. Windsor, C. Andreani, *Adv. Phys.*, 34(1985), 73
23. J. S. Sun, C. S. Wu, *Mater. Sci. Eng.*, 9(2001), 25
24. Y. Li, J. Wang, P. Liu, *Mater. Sci.*, 26(2003), 273
25. Z. Zengda, L. Yajiang, Y. Shike, *J. Mater. Sci. Technol.*, 15(1999), 555
26. R. ARicks, P. R. Howell, G. S. Barritte, *J. Mater. Sci.*, 17(1982), 732
27. K. Banerjee, U. K. Chatterjee, *Br. Cor. J.*, 35(2000), 273
28. E. A. Metzbower, J. Stoop, C. T. Fujii, F. W. Fraser, *J. Met.*, 10(1978), 15
29. K. Banerjee, U. K. Chatterjee, *Mater. Sci. Technol.*, 16(2000), 517
30. R. Venkatesan, PhD Thesis, *Department of metallurgy Indian institute of science*, 2000.
31. D. E. J. Talbot, J. D. R. Talbot. *Corrosion science and technology*, CRC Press, USA (1998).
32. R. Venkateshan, M. A. Venkatasamy, T. A. Bhaskaran. *Br. Corros. J.*, 37 (2002), 257
33. Z. Lu, Tetsuo Shoji, T. Dan, Y. Qju, T. Yonezawa, *Corros, Sci.*, 52 (2010), 2547
34. Z. Lu, T. Shoji, Y. Ito, A. Kai, N. Tsuchiya. *Corros, Sci.*, 50 (2008), 625
35. A. Turnbull, S. Zhou, G. Hinds. *Corros, Sci.*, 46 (2004), 193
36. A. Contreras, A. Albiter, M. Salazar, R. Perez, *Mater. Sci. Eng. A.*, 407 (2005), 45
37. E. Barsoukov, J. Ross Macdonald, *Impedance Spectroscopy Theory, Experiment, and Applications*, John Wiley & Sons, Inc., Hoboken, New Jersey, Canada (2005).
38. Z. Lu, T. Shoji, Y. Takeda, Y. Ito, A. Kai, S. Yamazaki., *Corros. Sci.* 50 (2008), 561
39. R. E. Melchers, R. Jeffrey, *Corros. Sci.*, 47 (2005), 1678
40. W.Y. Maeng, D. D. Macdonald. *Corros. Sci.* 2008, 50, 2239.